

QCD critical region and higher moments for three flavor models

B.-J. Schaefer^{1,2,*} and M. Wagner^{3,†}

¹*Institut für Theoretische Physik, Justus-Liebig-Universität Giessen, D-35392 Giessen, Germany*

²*Institut für Physik, Karl-Franzens-Universität Graz, A-8010 Graz, Austria*

³*Fakultät für Physik, Universität Bielefeld, D-33615 Bielefeld, Germany*

(Dated: June 21, 2018)

One of the distinctive features of the QCD phase diagram is the possible emergence of a critical endpoint. The critical region around the critical point and the path dependency of the critical exponents are investigated within effective chiral $(2+1)$ -flavor models with and without Polyakov loops. Results obtained in no-sea mean-field approximations where a divergent vacuum part in the fermion-loop contribution is neglected are compared to the renormalized ones. Furthermore, the modifications caused by the backreaction of the matter fluctuations on the pure Yang-Mills system are discussed. Higher-order, non-Gaussian moments of event-by-event distributions of various particle multiplicities are enhanced near the critical point and could serve as a probe to determine its location in the phase diagram. By means of a novel derivative technique higher-order generalized quark-number susceptibilities are calculated and their sign structure in the phase diagram is analyzed.

PACS numbers: 12.38.Aw, 11.10.Wx, 11.30.Rd, 12.38.Gc

I. INTRODUCTION

Two important properties of the QCD vacuum are spontaneous chiral symmetry breaking and color confinement. It is expected that chiral symmetry can be restored and that a confinement/deconfinement transition occurs at high temperature and/or baryon densities [1]. A deeper understanding of how these phase transitions manifest themselves both theoretically and experimentally is of utmost importance in mapping the phase diagram [2].

A crossover transition at vanishing density seems to be well established by recent QCD lattice simulations at almost physical quark masses. With a better continuum extrapolation and improved actions the latest value of the chiral critical temperature $T_\chi \approx 154 \pm 9$ MeV by the HotQCD Collaboration [3] is in agreement with $T_\chi \approx 147 - 157$ MeV of the Wuppertal-Budapest group [4]. However, the extrapolations of lattice simulations towards finite chemical potential are much under debate. Most theoretical model studies evidence a genuine second-order critical endpoint (CEP) where the first-order chiral phase transition line at large chemical potential terminates [5, 6]. Many properties of the endpoint such as, e.g., its exact location remain unknown. QCD lattice simulations cannot directly access the relevant region in the phase diagram but extensions towards finite chemical potential provide some limitations and can rule out the existence of a CEP for small μ/T ratios [7]. This observation agrees with recent first-principle QCD studies performed with functional renormalization group techniques and Dyson-Schwinger equations [8–10]. Moreover, the predicted chiral first-order transition at

small temperatures is model dependent. For example, the inclusion of the 't Hooft anomaly in chiral models may change the first-order transition to a smooth crossover [11].

This underlines the importance of the planned facilities such as the Compressed Baryonic Matter (CBM) experiment at the Facility for Antiproton and Ion Research (FAIR) and the Nuclotron-Based Ion Collider Facility (NICA) at the Joint Institute for Nuclear Research (JINR) and of the recently started "beam energy scan" at the Relativistic Heavy Ion Collider (RHIC, Brookhaven National Laboratory) [12] which are dedicated to search for a critical point. For an experimental overview see e.g. [13]. The knowledge of the characteristic signatures of the conjectured CEP is inevitable for the experiments [14, 15]. Possible experimental signatures which are based on the singular behavior of thermodynamic functions near a critical point were already suggested a decade ago (see, e.g., [16]). They are related to temperature and chemical potential fluctuations in event-by-event fluctuations of various particle multiplicities [17]. By scanning the center of mass energy and thus the baryochemical potential an increase and then a decrease in the number fluctuations of, e.g., pions and protons should be seen as one crosses the critical point. The nonmonotonic behavior in the number fluctuations in the vicinity of a critical point might serve as a probe to determine its location in the phase diagram assuming that the signals are not washed out by the expansion of the colliding system [18].

In a realistic heavy-ion collision the correlation length is cut off by critical slowing down and finite volume effects. In addition, the system has only a finite time to build up correlations. Estimates of the largest correlation length as the collision cools past the critical point are in the range of a few $(2 - 3)$ fm and only a factor 3 larger than the natural scale $(0.5 - 1)$ fm far away from the critical point [19]. Hence, if the correlation length

* bernd-jochen.schaefer@uni-graz.at

† mwagner@physik.uni-bielefeld.de

increases only by a few percent near a critical point more sensible quantities are needed for the analysis of freeze-out and critical conditions in heavy-ion collisions [20, 21]. Possible candidates are higher-order cumulants or ratios of higher-order generalized susceptibilities which depend on higher powers of the correlation length ξ . An example is the fourth-order susceptibility χ_4 which scales like ξ^7 near the critical point; hence, an enhancement by a factor 2 is expected for this quantity. The sign of the fourth moment should also change as the CEP is approached from the crossover side as pointed out in Ref. [22].

In this work we investigate the sign structure not only of the fourth moment (kurtosis) but also of higher-order moments in the (T, μ) phase diagram. We discuss the generic behavior of these higher moments at nonvanishing chemical potential within $(2+1)$ -flavor quark-meson (QM) and Polyakov-quark-meson (PQM) models which we briefly recapitulate in Sec. II. The no-sea mean-field findings are compared to the results obtained in the renormalized models. As mentioned in [23, 24] the critical region around the critical point in the phase diagram is not pointlike but has a richer structure. In Sec. III we investigate the size of the critical region and the path dependency of the critical exponents towards the critical point. The influence of the backreaction of matter fluctuations on the pure Yang-Mills system on the critical region is analyzed. In Sec. IV different ratios of moments of the baryon number fluctuations to high orders are calculated by means of a novel derivative technique [25]. We conclude and point out some experimental consequences from these findings in Sec. V.

II. THREE-FLAVOR MODELS

Chiral symmetry and its spontaneous breaking for three flavor is very well described by renormalizable quark-meson type models which serve as an effective realization of low-energy strongly-interacting matter [26]. These models can be augmented with the Polyakov loop (see, e.g., [27, 28]), yielding the PQM models which mimic in addition to the chiral symmetry breaking certain aspects of a statistical confinement.

The Lagrangian of the three-flavor ($N_f = 3$) PQM model [29] is assembled from three parts

$$\mathcal{L}_{\text{PQM}} = \bar{q} (i\mathcal{D} + h\phi_5 + \gamma_0\mu_f) q + \mathcal{L}_m - \mathcal{U}(\Phi, \bar{\Phi}), \quad (1)$$

where the first term describes the interaction between the $N_c = 3$ color quark fields $q = (u, d, s)$ and the mesons $\phi_5 = T_a(\sigma_a + i\gamma_5\pi_a)$ with a flavor-blind Yukawa coupling h . By T_a the nine generators of the $U(3)$ symmetry are denoted and σ_a (π_a) labels the (pseudo)scalar meson nonets. For each flavor $f \in \{u, d, s\}$ an independent quark chemical potential μ_f is introduced but in this paper we will consider symmetric quark matter with one uniform quark chemical potential $\mu \equiv \mu_B/3$. The quarks are coupled to a temporal, spatially constant background gauge field A_0 , which is represented

in terms of the Polyakov loops, via a covariant derivative $\mathcal{D} = \partial - i\gamma_0 A_0$. A gauge coupling has been absorbed in the gauge fields.

The second part in the Lagrangian, \mathcal{L}_m represents the purely mesonic contribution with the field $\phi = T_a(\sigma_a + i\pi_a)$ and reads

$$\begin{aligned} \mathcal{L}_m = & \text{Tr} (\partial_\mu \phi^\dagger \partial^\mu \phi) - m^2 \text{Tr} (\phi^\dagger \phi) - \lambda_1 [\text{Tr} (\phi^\dagger \phi)]^2 \\ & - \lambda_2 \text{Tr} (\phi^\dagger \phi)^2 + c (\det(\phi) + \det(\phi^\dagger)) \\ & + \text{Tr} [H(\phi + \phi^\dagger)] . \end{aligned} \quad (2)$$

The last term in Eq. (2) breaks chiral symmetry explicitly where $H = T_a h_a$ has in general nine external parameters h_a whereof only two are nonvanishing for a $(2+1)$ -flavor symmetry breaking pattern. The $U(1)_A$ symmetry is broken explicitly by the 't Hooft determinant with a constant strength c .

The last part of Eq. (1) represents the effective gluon field potential in terms of the Polyakov-loop variables Φ and $\bar{\Phi}$ [30] which approximate the dynamical glue sector of QCD. For vanishing chemical potential the bulk thermodynamics of lattice Yang-Mills is reproduced up to twice the deconfinement phase transition temperature [29, 31, 32]. Several explicit choices of the Polyakov-loop potential are known in the literature [28, 33, 34], see [29] for a comparison. In this work we employ the logarithmic version [33]

$$\begin{aligned} \frac{\mathcal{U}_{\log}}{T^4} = & -\frac{a(T)}{2} \bar{\Phi} \Phi \\ & + b(T) \ln \left[1 - 6\bar{\Phi} \Phi + 4(\Phi^3 + \bar{\Phi}^3) - 3(\bar{\Phi} \Phi)^2 \right] , \end{aligned} \quad (3)$$

with temperature-dependent coefficients

$$a(T) = a_0 + a_1 \left(\frac{T_0}{T} \right) + a_2 \left(\frac{T_0}{T} \right)^2, \quad b(T) = b_3 \left(\frac{T_0}{T} \right)^3$$

and the parameters $a_0 = 3.51$, $a_1 = -2.47$, $a_2 = 15.2$ and $b_3 = -1.75$ [29]. Originally, the parameter T_0 is fitted to the critical temperature $T_0 = 270$ MeV of the first-order deconfinement transition of the quenched $SU(3)$ lattice gauge theory.

However, in full dynamical QCD the effective Polyakov-loop potential has to be replaced by the corresponding QCD Yang-Mills (YM) part. Within a functional renormalization group approach the critical temperature of the quenched YM system could be determined recently [35]. Because of the matter fluctuations the glue propagation is further dressed (see also [9]). A first phenomenological hard thermal loop estimate for this flavor and chemical potential dependence of the critical temperature has been given in [36] and within perturbation theory (see [37]). These considerations demonstrate that low-energy models such as the PQM model can be understood as a specific approximation of QCD and can be systematically enhanced towards full dynamical QCD.

To be more specific: the matter backreaction to the gluon sector leads to N_f and μ modifications in T_0 , i.e., $T_0 \rightarrow T_0(N_f, \mu)$ as introduced in [36] (see also [8, 29, 37, 38] for more details).

Explicitly, we employ

$$T_0(N_f, \mu) = T_\tau e^{-1/(\alpha_0 b(N_f, \mu))} \quad (4)$$

where $T_\tau = 1.77$ GeV denotes the τ scale and $\alpha_0 = \alpha(\Lambda)$ the gauge coupling at some UV scale Λ . The μ -dependent running coupling reads

$$b(N_f, \mu) = b(N_f) - b_\mu \frac{\mu^2}{T_\tau^2}, \quad (5)$$

with the factor $b_\mu \simeq \frac{16}{\pi} N_f$.

Finally, the grand potential in mean-field approximation (MFA) is the sum of three terms consisting of the meson, U , the fermion-loop contribution $\Omega_{\bar{q}q}$, evaluated in the presence of the Polyakov loop and the pure gauge

field contribution, the Polyakov-loop potential \mathcal{U} :

$$\Omega = U(\sigma_x, \sigma_y) + \Omega_{\bar{q}q}(\sigma_x, \sigma_y, \Phi, \bar{\Phi}) + \mathcal{U}(\Phi, \bar{\Phi}). \quad (6)$$

Φ and $\bar{\Phi}$ denote the real Polyakov-loop expectation values and σ_x and σ_y are the light and strange chiral condensates in the rotated nonstrange-strange basis (see [39] for further details). The temperature and density behavior of the four order parameters is obtained by minimization of the grand potential Eq. (6). Explicitly, the mesonic part reads

$$U(\sigma_x, \sigma_y) = \frac{m^2}{2} (\sigma_x^2 + \sigma_y^2) - h_x \sigma_x - h_y \sigma_y - \frac{c}{2\sqrt{2}} \sigma_x^2 \sigma_y^2 + \frac{\lambda_1}{2} \sigma_x^2 \sigma_y^2 + \frac{1}{8} (2\lambda_1 + \lambda_2) \sigma_x^4 + \frac{1}{8} (2\lambda_1 + 2\lambda_2) \sigma_y^4, \quad (7)$$

with six parameters $m^2, c, \lambda_1, \lambda_2, h_x, h_y$ and the quark-antiquark contribution in the presence of the Polyakov loop accordingly

$$\begin{aligned} \Omega_{\bar{q}q}(\sigma_x, \sigma_y, \Phi, \bar{\Phi}) = -2 \sum_{f=u,d,s} \int \frac{d^3p}{(2\pi)^3} \left\{ N_c E_{q,f} + T \ln \left[1 + 3(\Phi + \bar{\Phi} e^{-(E_{q,f} - \mu_f)/T}) e^{-(E_{q,f} - \mu_f)/T} + e^{-3(E_{q,f} - \mu_f)/T} \right] \right. \\ \left. + T \ln \left[1 + 3(\bar{\Phi} + \Phi e^{-(E_{q,f} + \mu_f)/T}) e^{-(E_{q,f} + \mu_f)/T} + e^{-3(E_{q,f} + \mu_f)/T} \right] \right\} \quad (8) \end{aligned}$$

with the flavor-dependent single-particle energies

$$E_{q,f} = \sqrt{p^2 + m_f^2} \quad (9)$$

and quark masses $m_l = h\sigma_x/2$ and $m_s = h\sigma_y/\sqrt{2}$. The first term in quark/antiquark-loop contribution $\Omega_{\bar{q}q}$, Eq. (8), represents the ultraviolet divergent vacuum contribution. It is neglected in the no-sea MFA but can be renormalized with, e.g., the dimensional regularization scheme yielding

$$\Omega_{\bar{q}q}^{\text{vac}}(\sigma_x, \sigma_y) = -\frac{N_c}{8\pi^2} \sum_{f=u,d,s} m_f^4 \log\left(\frac{m_f}{\Lambda}\right) \quad (10)$$

where the regularization scale Λ has been introduced. Note that the Λ dependence is completely absorbed by the mesonic potential U . Hence all thermodynamic quantities are finally independent of the choice of the regularization scale at the mean-field level. With this term fermion fluctuations are taken into account whereas meson fluctuations are still ignored. A careful investigation of the influence of this vacuum term in two-flavor model studies can be found in [40–42] and recently for a $(2+1)$ -flavor PQM model in [29]. To disentangle physical effects driven by fluctuations we will compare no-sea mean-field results with the renormalized ones where this term has been taken into account.

The parameters of the model, Eq. (1), are chosen to reproduce experimentally known quantities like the pion and kaon decay constants and the scalar and pseudoscalar meson masses. The only insecure and not precisely known quantity is the sigma mass which influences the phase structure [29]. To compare with previous works [39] we choose $m_\sigma = 600$ MeV for the no-sea mean-field approximation and $m_\sigma = 400$ MeV for the renormalized model (see also the next section).

Neglecting the Polyakov-loop potential in Eq. (6) and the background gauge field A_0 in the covariant derivative which corresponds to $\Phi = \bar{\Phi} = 1$ in the quark contribution Eq. (8) results in the corresponding three-flavor quark-meson model. Since the Polyakov loop decouples from the QM sector in the vacuum no parameter adjustments are necessary.

III. PHASE STRUCTURE AND THE CRITICAL ENDPOINT

In Fig. 1 the $(2+1)$ -flavor chiral phase diagrams for the QM and the PQM models with and without the matter backreaction via $T_0(\mu)$ are presented in no-sea mean-field approximation [1(a)] and in the renormalized models [1(b)]. The crossover in the strange sector which takes place at higher temperatures is not shown. The almost

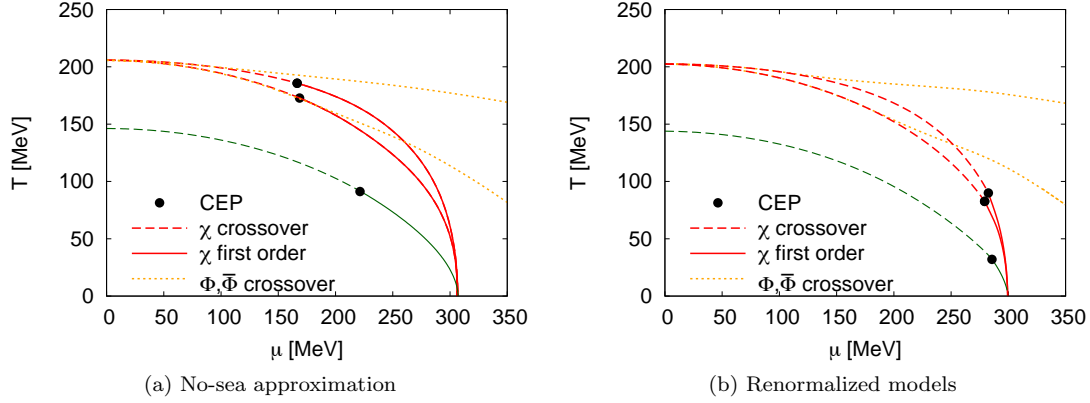


FIG. 1. Three-flavor chiral phase diagrams [upper lines, PQM models for a constant T_0 (top line) and for $T_0(\mu)$; lower lines, QM models]. (a) No-sea MFA with $m_\sigma = 600$ MeV; (b) renormalized models with $m_\sigma = 400$ MeV. The peak in the temperature derivative of the Polyakov loops Φ , $\bar{\Phi}$ is also shown (light dashed lines).

degenerated positions of the peaks of the temperature derivative of both Polyakov loops Φ and $\bar{\Phi}$ are indicated by the light dashed lines.

In all models the vacuum term in the grand potential moves the location of the endpoint away from the T axis towards the μ axis whereas the Polyakov loop increases the chiral transition temperature at $\mu = 0$ and hence moves the CEP back to higher temperatures. For example the PQM model in no-sea approximation without the matter backreaction for a constant $T_0 = 270$ MeV yields a CEP at $(T_c, \mu_c) = (186, 167)$ MeV which changes to $(T_c, \mu_c) = (172, 169)$ MeV if the matter backreaction is taken into account. Without the Polyakov loop the CEP lies at $(T_c, \mu_c) = (92, 221)$ MeV. With vacuum fluctuations the location of the CEP changes significantly to $(T_c, \mu_c) = (90 (83), 283 (280))$ MeV in the renormalized PQM model without (with) matter backreaction. In the renormalized QM model the CEP lies close to the μ axis at $(T_c, \mu_c) = (32, 286)$ MeV.

The location and hence the existence of a CEP in the phase diagram is sensitive to the sigma meson mass m_σ [39, 43]. A larger m_σ in general pushes the CEP towards the μ axis. Already for $m_\sigma = 600$ MeV the CEP disappears in the renormalized models (see also [29, 39]). We have adapted $m_\sigma = 400$ MeV in the renormalized models such that a common value for the chiral transition of $T_\chi \approx 205$ MeV at $\mu = 0$ is secured as in the no-sea mean-field approximation.

In the PQM models the coincidence of the chiral and deconfinement transitions extends to larger chemical potentials if the backreaction to the YM sector is implemented via Eq. (4). Thus, the inclusion of fluctuations and the matter back-coupling to the YM sector reduces a possible chirally symmetric and confining region in the phase diagram as found in a large- N_c limit study [44]. A similar result is obtained if one goes beyond mean field with, e.g., functional techniques such as the functional renormalization group [8] or Dyson-Schwinger equations

[10] where both transitions coincide over the whole phase diagram. Hence, the inclusion of the μ dependence in T_0 in the Polyakov-loop potential represents a further step beyond the standard mean-field approximation. However, at vanishing temperature all transitions collapse to the same critical μ and the Polyakov loop does not influence the chiral sector. Of course, in this domain other degrees of freedom like baryons, which are usually neglected in such (P)QM- or (P)NJL-type model studies, become more important which we do not address here.

A. Anatomy of the critical region

The knowledge of the size of the critical region around the CEP in the phase diagram is important for the experimental detection of the endpoint in heavy-ion collisions. The region is obtained as a projection of different constant ratios

$$R = \frac{\chi_q}{\chi_q^{\text{free}}} \quad (11)$$

of the quark-number susceptibility χ_q normalized with the free susceptibility χ_q^{free} onto the (T, μ) -plane near the CEP. In Fig. 2 three ratios R , obtained in no-sea MFA, are plotted as contours relative to the endpoint. Compared to the QM model (right panel) the Polyakov loop compresses the critical region, in particular in the T -direction. With the matter back-coupling (solid lines) this effect is weaker and the region is twice as large in the T -direction. In μ -direction the modification is even less pronounced. Without the matter back-coupling the chiral and deconfinement transition deviate already in the vicinity of the CEP. As a consequence the quark determinant is more suppressed near the chiral transition and hence the size of the critical region.

The effect of the vacuum contribution in the grand potential on the size of the critical region is shown in Fig. 3.

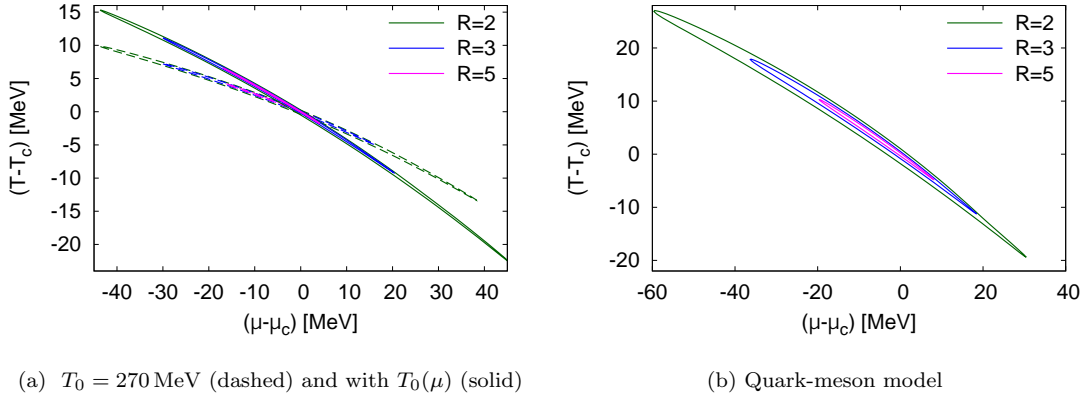


FIG. 2. The critical region around the CEP for three different three-flavor models in no-sea MFA: PQM model with a logarithmic Polyakov-loop potential and constant and running T_0 (a) and the QM model (b). See text for details.

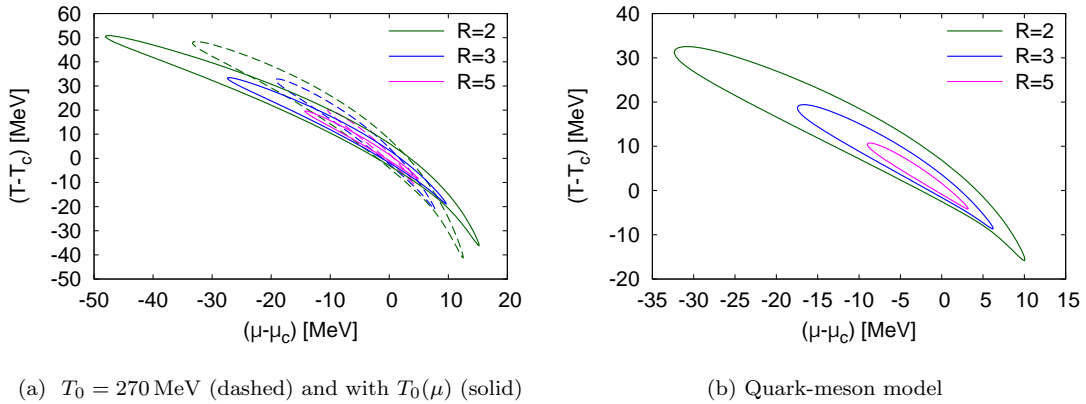


FIG. 3. The critical region similar to Fig. 2 for the corresponding renormalized models.

The incorporated fluctuations increase the critical region in direction perpendicular to the crossover line in the phase diagram. This effect is more prominent in the QM model without the Polyakov loop [3(b)]. The Polyakov loop affects the critical region less than in the no-sea approximation. However, the region in the renormalized PQM models [3(a)] is larger than in the renormalized QM model. This can be understood by the observation that the Polyakov loop modifies the quark determinant mostly at moderate chemical potentials. In the renormalized models the CEP is located at larger chemical potentials around $\mu \approx 280 - 285$ MeV. Thus, the enhanced critical region with the Polyakov loop results also from the higher critical temperature [cf. also Fig. 1(b)]. The matter backreaction modifies the critical region in a similar fashion as in the no-sea approximation.

In general, fluctuations wash out the phase transition and the chiral crossover is much smoother. As a consequence, the size of the critical region becomes broader in direction perpendicular to the extended first-order transition line. But due to the shift of the endpoint away from the T -axis the size of the critical region turns out to be

smaller along the phase boundary compared to the no-sea MFA. Furthermore, for larger chemical potentials and smaller temperatures the influence of the Polyakov loop becomes insignificant and hence the size of the critical region becomes comparable in both renormalized models.

All critical regions exhibit an elongation along the direction parallel to the first-order phase transition line. The peak of the quark-number susceptibility follows the crossover line and diverges at the CEP. The divergence is described by a power law within the critical region. The shape of the critical region is induced by the path dependency of the corresponding critical exponents near the singularity as already pointed out in [45]. One reason for the elongation of the critical region in a direction parallel to the first-order line is that the corresponding critical exponent is larger [24, 46].

This behavior is elucidated in the following: In Fig. 4 a generic plot of the region near the CEP in the phase diagram with three different paths towards the CEP, labeled with A, B and C (A' , B' and C') for $\hat{t} > 0$ ($\hat{t} < 0$) where $\hat{t} \equiv (T - T_c)/T_c$ is shown. Path A (A') is chosen such that it is parallel to the (extended) first-order

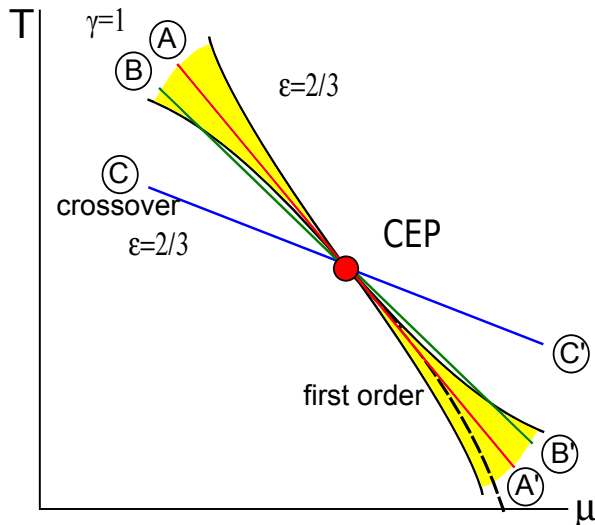


FIG. 4. Schematic plot of three different paths (labeled with A, B and C and with A', B' and C') towards the CEP in the phase diagram. The yellow-shaded inner regions denote the area parallel to the (extended) first-order line (dashed) where the critical exponent of the quark-number susceptibility deviates from the one outside this area. See text for details.

line. It corresponds to the Ising model temperaturelike direction with a vanishing "magnetic field" component in the sense of Griffiths and Wheeler [45]. The remaining paths B (B') and C (C') do have some additional "magnetic field" contributions. For the critical exponent ϵ , which is defined by

$$\chi_q \propto r^{-\epsilon} \quad (12)$$

with the reduced distance

$$r = \sqrt{\hat{t}^2 + \hat{\mu}^2} \quad (13)$$

from the CEP with $\hat{\mu} = (\mu - \mu_c)/\mu_c$, two different scaling regions can be distinguished. The explicit form and size of these regions are not universal. They depend on the used thermodynamic variables and the underlying equation of state; however, the mapping is analytic [45]. When the T, μ variables are used, the inner region is very small. For the outer and larger region, perpendicular to the extended first-order line, the mean-field value $\epsilon = 2/3$ is found. Within a narrow area, parallel to this first-order line, a value of $\gamma = 1$ is seen which corresponds to the Ising temperature-like exponent for vanishing external field $\gamma = \epsilon\beta\delta = 1 > \epsilon$ (cf. Fig. 4). The critical exponent does not depend on whether one approaches the critical point from the side with $\hat{t} > 0$ or from $\hat{t} < 0$. The scaling behavior is confirmed and demonstrated in Fig. 5 where the logarithm of the quark-number susceptibility for three different paths towards the CEP (for $\hat{t} > 0$) as a function of the logarithm of the reduced distance r is presented.

In the figure the scaling of the susceptibility for the PQM model without $T_0(\mu)$ corrections (left panel) and

Path	$T_0 = 270 \text{ MeV}$	$T_0(\mu)$
$\hat{t} > 0$	0.669 ± 0.002	0.669 ± 0.002
$\hat{t} < 0$	0.662 ± 0.003	0.663 ± 0.002
$\hat{\mu} > 0$	0.667 ± 0.003	0.669 ± 0.002
$\hat{\mu} < 0$	0.663 ± 0.002	0.662 ± 0.003
A'	1.00 ± 0.02	1.00 ± 0.02
A	1.01 ± 0.02	1.01 ± 0.02

TABLE I. Critical exponents of the quark-number susceptibility in the PQM model with a logarithmic Polyakov-loop potential for a constant and a running T_0 for different paths towards the CEP.

for the QM model (right panel) over several orders of magnitude is shown. The slope corresponds to the critical exponent. For the path B in the QM model one nicely recognizes the scaling crossing from the inner region with an exponent $\gamma = 1$ to the outer region with an exponent $\epsilon = 2/3$.

A similar scaling crossing in the slopes of the corresponding PQM curves is also visible in Fig. 5 with a small numerical uncertainty for path B very close to the CEP. The distance r where the crossing of the different scaling regimes in the figure takes place depends on the chosen angle of the path relative to the CEP coordinates. This crossing determines the boundary of the narrow yellow-shaded regime in Fig. 4. Summarizing the findings for both models, with and without the Polyakov loop, the inner regime tapers with a very small angle below 0.1 degrees.

The criticality is also not affected by the backreaction of the matter fluctuations to the YM sector. In Tab. I the critical exponents for paths parallel to the μ and T axes towards the CEP with and without the $T_0(\mu)$ corrections are listed. We find for these paths the expected mean-field critical exponent $2/3$ [47]. For the paths parallel to the first-order transition line (labeled with A and A') an exponent $\gamma = 1$ is obtained. If one goes beyond the no-sea mean-field approximation using the renormalized potentials, the critical exponents remain mean field since the universality is not modified.

IV. NON-GAUSSIAN FLUCTUATIONS

In a realistic heavy-ion collision the detection of the critical region, in particular of an endpoint, is hampered by a finite correlation length as argued in the introduction. When we approach a critical point more and more non-Gaussian components in the probability distribution of the corresponding order parameter are developed. The corresponding higher moments are much more sensitive on a diverging correlation length and thus seem to be a more appropriate tool to guide the experiment to locate an endpoint [48].

Fluctuations of conserved charges are quantified by cumulants in statistics which are directly related to generalized susceptibilities [14, 49–51]. They can be defined

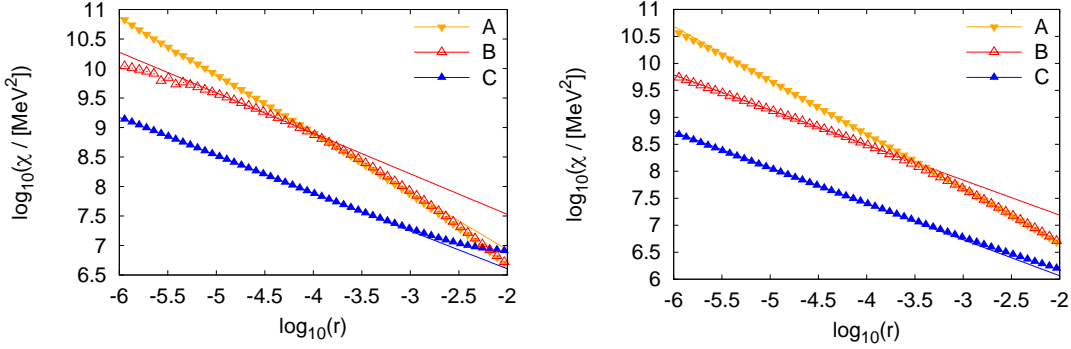


FIG. 5. The scaling of the quark-number susceptibility χ_q . Three different paths (cf. Fig. 4) towards the CEP are shown for the PQM model (left panel) and for the QM model (right panel) in no-sea MFA.

as derivatives of the logarithm of the partition function with respect to the appropriate chemical potentials. For three different chemical potentials we have accordingly

$$\chi_{n_i, n_j, n_k} \equiv \frac{1}{VT} \frac{\partial^{n_i}}{\partial (\mu_i/T)^{n_i}} \frac{\partial^{n_j}}{\partial (\mu_j/T)^{n_j}} \frac{\partial^{n_k}}{\partial (\mu_k/T)^{n_k}} \log Z, \quad (14)$$

where n_i, \dots denotes the order of the derivatives and the indices $(i, j, k) = (u, d, s)$ the quark flavor.

The generalized susceptibilities evaluated at vanishing μ_f are the Taylor expansion coefficients of the pressure series in powers of μ_f/T . The coefficients and the convergence properties of the Taylor series were recently analyzed in a similar model study [52, 53]. Moreover, higher-order susceptibilities are also known up to eighth order from QCD lattice simulations [54, 55].

For the corresponding n th order moment of the quark-number fluctuations for one uniform quark chemical potential, we write χ_n . The ratio of different order susceptibilities is volume independent and can thus be directly linked to moment products of various baryon number distributions. Examples are the net-proton kurtosis κ and the variance σ which can be combined to $\kappa\sigma^2 = \chi_4/(9\chi_2)$ and the net-proton skewness S which can be expressed as $S\sigma = \chi_3/(3\chi_2)$. The factors arise because χ_n are the quark-number susceptibilities. These moments establish a deeper connection between theoretical predictions and experimental measurements: only in the vicinity of the CEP might the products $\kappa\sigma^2$ and $S\sigma$ show large deviations from its Poisson value. In the crossover regime at smaller chemical potentials, they are close to 1. Presently, these quantities are the subject of ongoing discussions [22, 56, 57]. Unfortunately, the existing statistics on the experimental side are not yet sufficient to draw any reliable conclusions which might point to the existence of a critical point in the phase diagram [58].

In the following we denote the n th to m th order moment ratio as

$$R_{n,m} \equiv \chi_n(T, \mu) / \chi_m(T, \mu), \quad (15)$$

such that, e.g., $\kappa\sigma/S = R_{4,3}/3$. The direct model evalu-

ation of $R_{n,m}$ becomes quickly cumbersome and tedious already for lower orders because the order parameters depend implicitly on the chemical potential.

The evaluation of the ratios can be automated by means of a novel numerical derivative technique, based on the algorithmic differentiation (AD) idea. With this technique derivatives of arbitrary order at machine precision can be obtained. Compared to other differentiation techniques such as the standard divided differentiation method or symbolic differentiation, the AD is faster and produces truncation-error-free derivatives of a given function. Details and a comprehensive introduction to the AD technique is given in [59]. Physics applications of this technique can be found at various places: The AD generalization to implicitly dependent functions which is also needed in this work was done in [25] and in [32] the Taylor coefficients to very high orders for a three-flavor model have been calculated for the first time at vanishing chemical potential. These findings confirm impressively the power and usability of this technique. In this work we extend this method to nonvanishing chemical potentials.

We begin with a discussion of the ratios $R_{n,2}$ with even $n \geq 4$. Since the moment χ_2 , i.e., the quark-number susceptibility, is always positive and continuous in the chiral crossover regime it cannot modify the sign structure of $R_{n,2}$ near the phase transition. Thus, the ratios $R_{n,2}$ are a suitable quantity to inspect the change of sign of all higher-order moments χ_n in the phase diagram.

The ratio $R_{4,2}$ measures basically the quark content of particles carrying baryon number. For vanishing quark chemical potential this ratio (if quark-number susceptibilities are used) tends to nine for low temperature and for high temperature to $6/\pi^2$ which follows immediately from the Stefan-Boltzmann limit. In a hadron resonance gas (HRG) model the ratio is temperature independent and all moments stay positive since the HRG has no phase transition with singularities. Hence, higher-order moments can differ significantly from a HRG calculation along the chemical freeze-out line even if the lower-order moments agree with HRG results and the thermodynam-

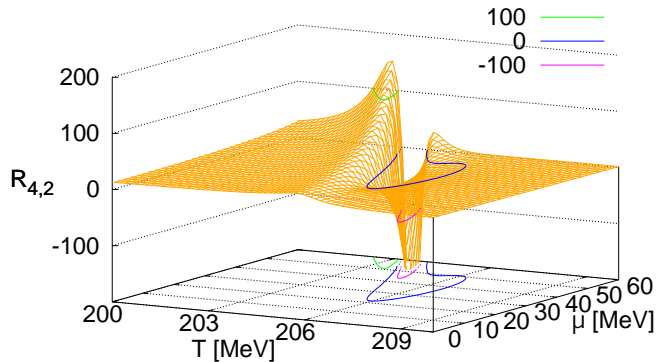


FIG. 6. The ratio $R_{4,2}$ in the PQM model with a constant T_0 .

ics and the particle yields at low temperature are well described by the HRG model [22, 43, 60]. Any deviation from the HRG model result might be an indicator for a real critical phenomenon (in equilibrium) and thus serves as a theoretical baseline for the analysis of heavy-ion collisions [22, 52].

In Fig. 6 the ratio $R_{4,2}$ calculated in the PQM model in no-sea MFA with a constant T_0 around the crossover region is shown. The contour lines projected onto the temperature and chemical potential plane are close to the chiral crossover line in the phase diagram. One clearly recognizes the development of a negative region for non-vanishing chemical potentials. These three-flavor results differ from a two-flavor mean-field calculation with and without the vacuum term [41]. Without the vacuum term the two-flavor kurtosis develops a peak at $\mu = 0$ near the crossover which is a remnant of the first-order transition in the chiral limit [61]. The fermion vacuum term changes the transition to second-order in the chiral limit consistent with universality arguments [62, 63]. For three massless flavor a first-order transition always emerges in the chiral limit with or without the vacuum term. The peak of the kurtosis for physical pion masses is already less pronounced in the no-sea mean-field approximation. This suppression at $\mu = 0$ is caused by the strange quarks and not by fluctuations (cf. Fig. 7 in [29]). Including the vacuum term the peak in the kurtosis finally vanishes also for the three-flavor case.

The higher moments start to oscillate within a narrow temperature interval for temperatures near the chiral transition [32]. The structures of all moments at $\mu = 0$ are related to each other and the behavior including the amplitudes of χ_n can be estimated by the temperature derivative of χ_{n-2} [53]. In contrast to the HRG model the ratios in our calculation become negative in the vicinity of the crossover for nonvanishing chemical potential as shown in Fig. 6. Since the fourth-order moment χ_4

is unaffected by chiral critical phenomena at vanishing chemical potential it remains positive for $\mu < 20$ MeV. This changes for larger chemical potentials since then nontrivial contributions from higher-order moments evaluated at $\mu = 0$ emerge and induce the change of sign in the ratios [51, 64]. This can be seen explicitly by a Taylor expansion of the corresponding moment around $\mu = 0$.

Higher-order ratios behave in a similar way [32, 51]. In Fig. 7 the negative regions of several ratios $R_{n,2}$ along the chiral crossover line are compared to each other for two models in no-sea MFA. All negative regions are closely correlated with the crossover curve. For ratios with $n > 4$ the negative regions are shifted slightly away from the crossover curve in the hadronic phase and all regions converge exactly at the CEP. The Polyakov loop sharpens the size of the negative region in the phase diagram.

The effect of the vacuum fluctuations on the negative regions is demonstrated in Fig. 8 where similar to the previous Fig. 7 the results of various even $R_{n,2}$ ratios with the corresponding renormalized models are shown. The CEP is pushed towards higher chemical potentials and the crossover is washed out by fluctuations. The curvature of the crossover line seems not to be changed. The effect of the fluctuations is drastic in the renormalized quark-meson model [8(b)] but not so large when the Polyakov loop is considered [8(a)].

We conclude that the negative fluctuations can surely be attributed to critical dynamics. Furthermore, these findings underline once more the importance of fluctuations. Generically, one observes that all regions calculated in the renormalized models are shifted more in the hadronic phase.

The appearance of negative values in χ_n at $\mu = 0$ has already been suggested as a criterion to determine the chiral critical temperature with Taylor expansion methods in lattice simulations. For example, the $\mu = 0$ values of Fig. 7(a) correspond to the ones in Fig. 5 of Ref. [53]. However, the critical temperature estimated with this criterion deviates strongly from the chiral critical one. The knowledge how the negative regions evolve towards the endpoint might be used to construct new criteria to improve the T_c estimate from a Taylor expansion around $\mu = 0$.

We close this section with a discussion of $R_{n,2}$ for odd integers n which have not been addressed in the literature so far. They vanish at $\mu = 0$ for all temperatures due to the CP symmetry of the QCD partition function and change sign at the endpoint. The quark-number density $n_q/T^3 = \chi_1$ is always positive for nonvanishing chemical potential. Hence, negative values can only be found at finite μ/T for $n \geq 3$. The emergence of the first zero in the ratios is similarly related to the chiral phase boundary as previously discussed for the even ratios. It is instructive to define the distance $\Delta T = T_n - T_\chi$ of the first zero in temperature direction of the ratio $R_{n,2}$ to the crossover temperature T_χ . In Fig. 9 the distance ΔT of four different ratios $R_{n,2}$ is plotted as a function of μ/T in no-sea MFA. All curves in the figure start at $\mu/T \approx 0$ except the

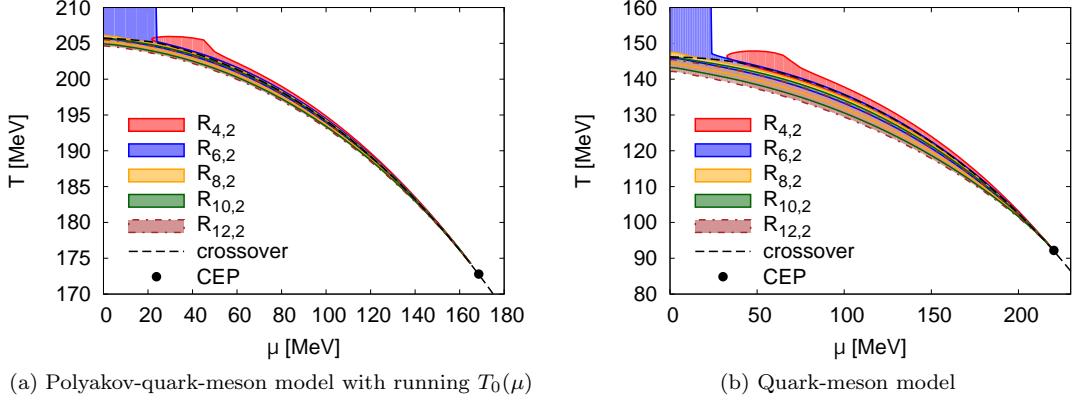


FIG. 7. Negative regions of the ratios $R_{n,2}$ along the crossover line in the phase diagram.

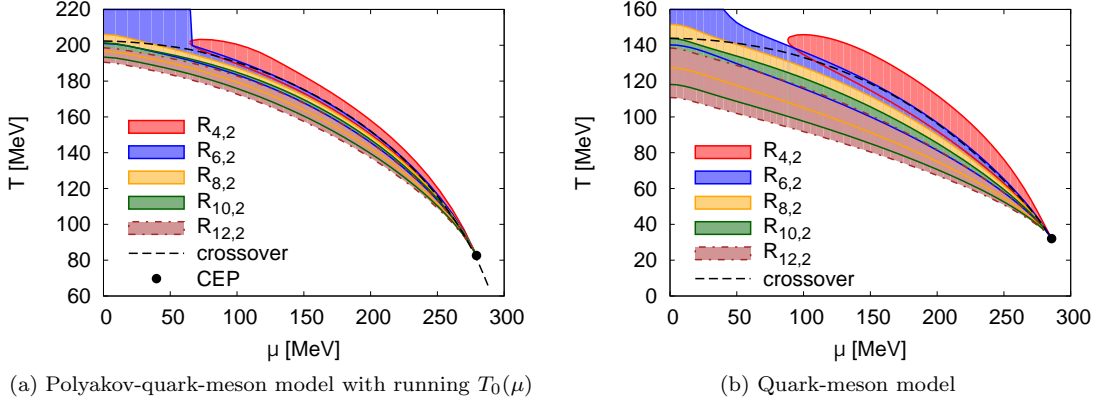


FIG. 8. Negative regions similar to Fig. 7 for the corresponding renormalized models.

one for the ratio $R_{3,2}$ which is positive at small chemical potentials. All curves obey a minimum whose location and depth depend on the model and used approximation. This is clearly visible in the next Fig. 10 where the vacuum term has been included. For completeness we have also added some even ratios in the figure which behave very similar to the odd ratios. Thus our considerations are not restricted to odd ratios.

For the PQM model [10(a)] the negative regions are closer to the crossover line than for the QM model [10(b)]. All curves converge to the CEP. All distances are negative for $n \geq 5$ meaning that the first zero in the ratio $R_{n,2}$ is pushed in the hadronic phase. The ratio $R_{3,2}$ stays close to the crossover line and becomes negative only in the vicinity of the CEP, in particular when the vacuum term is included, cf. Fig. 10. For this case the minimum is deeper by almost a factor of 10 due to the smoothening of the crossover driven by fluctuations. On the other hand, the Polyakov loop sharpens the transitions and consequently the minimum is not as deep (a factor 4 smaller) as in the QM model.

An interesting observation is the almost linear behavior of ΔT for intermediate μ/T ratios in both models with

and without the vacuum term and for all ratios. The linear extrapolation of ΔT from intermediate μ/T ratios to larger ratios where ΔT vanishes might serve as an estimator for the proximity of the thermal freeze-out to the crossover line and the existence of a possible endpoint can be ruled out for smaller μ_c/T_c ratios. Of course, due to some nonlinearities near the CEP this is only a lower bound for μ/T . The deviations from the linear behavior are yet smaller in the more realistic PQM model in contrast to the QM model (cf. Fig. 10). This estimate could be strengthened by considering only the difference of the subsequent roots in the odd ratios which is independent of the chiral crossover temperature. In Fig. 11 the relative temperature distance $\Delta\tau \equiv T_{n+2} - T_n$ for several odd integers is shown as a function of μ/T without the vacuum term. The curves exhibit a similar behavior as in Fig. 9 except for the ordering of the curves with respect to n . With increasing n the distance between subsequent ratios decreases signaling a possible convergence of the negative regions in the phase diagram. An estimation of the lower bound of the CEP with a linear fit between $\mu/T = 0.4 \dots 0.7$ ($= 1.0 \dots 1.5$) for the PQM (QM) model in no-sea approximation yields already a

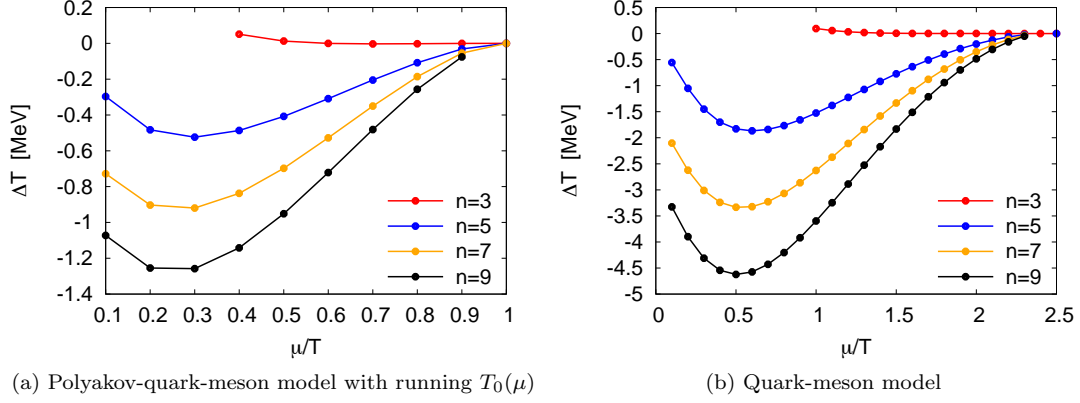


FIG. 9. Distance $\Delta T \equiv T_n - T_\chi$ of the first zero for various ratios $R_{n,2}$ to the chiral temperature T_χ as a function of μ/T in no-sea MFA.

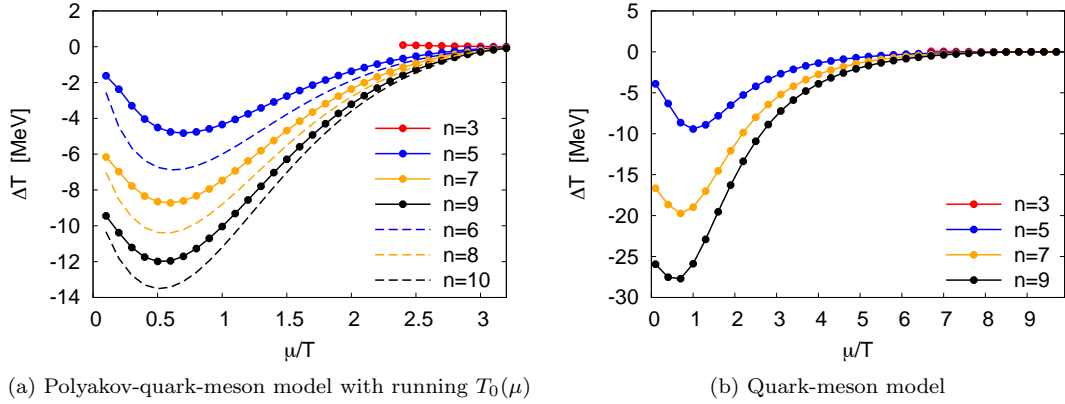


FIG. 10. Distance ΔT similar to Fig. 9 for the corresponding renormalized models.

critical $\mu_c/T_c \approx 0.9$ (2.0) for the lowest ratios ($n = 3$) which is quite close to the actual values $\mu_c/T_c \approx 1.0$ (2.4). For higher n these estimates become even better. Translating these numbers to the critical temperature yields $T_c \approx 175$ MeV (100 MeV) already for the lowest ratio $R_{3,2}$.

V. SUMMARY

In this work we addressed the role of fluctuations in three-flavor chiral (Polyakov-)quark-meson models and discussed their phenomenological consequences. The results obtained in no-sea mean-field approximations where an ultraviolet divergent part of the fermion-loop contribution to the grand potential is neglected were compared with findings of the corresponding cutoff-independent renormalized models. The influence of the vacuum term on the critical endpoint in the phase diagram, the size of the critical region around the endpoint and its criticality with respect to its effect on the universality in general were elucidated in detail. Because of the path

dependence of the critical exponent towards the critical endpoint, the critical region which we define as a projection of constant normalized quark-number susceptibilities on the (T, μ) plane is elongated in the direction of the crossover line. In the renormalized models a broadening perpendicular to the crossover line and simultaneously a shrinking in the direction of the chemical potential axis were found. The broadening is reduced if the Polyakov loop is taken into account. The Polyakov loop also shifts the crossover at vanishing chemical potential and consequently the critical endpoint to higher temperatures. On the other hand, in the renormalized models the location of the endpoint is pushed away from the temperature- towards the chemical potential axis which is a genuine effect of fluctuations. This shift can be compensated by reducing the experimentally insecure sigma meson mass in these models accordingly. In addition, the matter backreaction to the pure Yang-Mills sector in the Polyakov-quark-meson models which represents a further step beyond the mean-field approximation has also been implemented and the impact on the location of the endpoint and its critical region was analyzed. With the

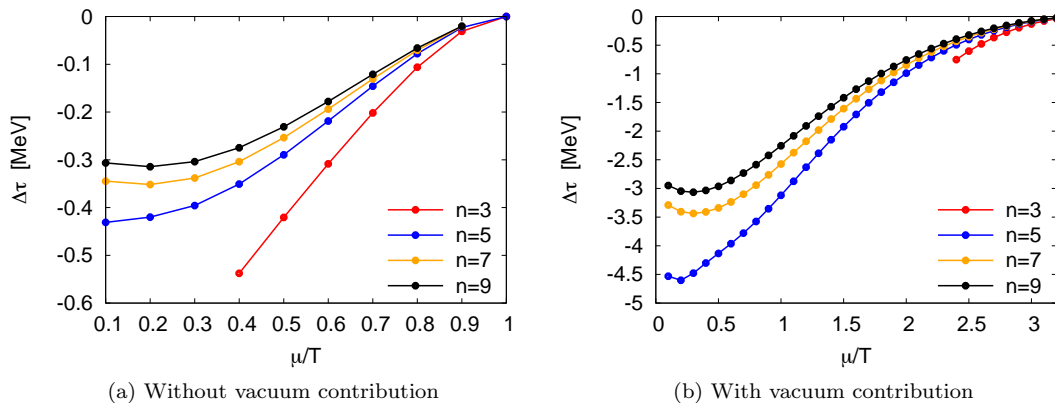


FIG. 11. Relative temperature distance $\Delta\tau \equiv T_{n+2} - T_n$ of the first zero in various subsequent odd ratios $R_{n,2}$ for the PQM model with running $T_0(\mu)$.

matter back-coupling improvement the chiral light phase transition and the peak in the temperature derivative of the Polyakov loops coincide over a larger region in the phase diagram when we synchronize both transitions at vanishing chemical potential by fixing the Polyakov-loop parameter T_0 . This coincidence increases even further when more fluctuations are taken into account as seen in recent functional renormalization group and Dyson-Schwinger calculations.

The scaling properties of the quark-number susceptibility in the vicinity of the endpoint are not modified by the fermion-loop vacuum fluctuations and a crossover phenomenon between two different scaling regimes was clearly seen. These regimes also determine the explicit shape of the critical region in the phase diagram which is not universal property but depends on the used thermodynamic variables and underlying equation of state.

As argued in the introduction, higher-order cumulants or generalized susceptibilities are more sensitive on the diverging correlation length and might be an appropriate quantity for the experimental search of an endpoint in the phase diagram. They are given as corresponding chemical potential derivatives of the partition function and are thus related to the Taylor expansion coefficients of the pressure series.

By applying a novel numerical derivative technique, we could calculate higher moments to very high orders at finite chemical potential. In contrast to the HRG model which does not have a phase transition with singularities, the kurtosis stays positive. In our models and independent of the used approximation the higher-order moments differ significantly from the HRG model result along the freeze-out curve due to the existence of an endpoint. As a consequence the ratios between various moments develop a negative region in the phase diagram close to the chiral transition line. Fluctuations smoothen the transitions and hence the ratios and the negative regions are broader and are shifted towards the hadronic phase in the renormalized models. All regions converge

at the endpoint.

In order to quantify this general trend we have introduced two new quantities: the distance of the first zero in temperature direction of various ratios to the crossover temperature and the relative distance between subsequent roots in the ratios which does not require the knowledge of the insecure chiral crossover temperature. Both quantities have a minimum as a function of the μ/T ratio. By using a linear extrapolation for intermediate μ/T ratios as an estimator we could rule out the existence of an endpoint for smaller μ/T ratios. This estimator might be useful for lattice simulations where only the negative regions for the first few ratios for small densities might be available.

An interesting difference to a corresponding two-flavor PQM calculation concerns the ratio $R_{4,2}$ at vanishing chemical potential: without the vacuum term the two-flavor kurtosis develops a peak at $\mu = 0$ near the crossover. The vacuum term smoothen the transition and the peak disappears finally. In the three-flavor calculation the peak is already suppressed in the no-sea approximation and hence is not driven by fluctuations.

It would be interesting to investigate higher moments of the so far neglected electric charge or strangeness fluctuations in particular beyond the mean-field level with the functional renormalization group. Work in this direction is ongoing.

Acknowledgments

We are grateful to Christian Fischer, Kenji Fukushima, Frithjof Karsch, Volker Koch and Krzysztof Redlich for valuable discussions. This work was supported by the BMBF Grant No. 06BI9001, the Helmholtz International Center for FAIR within the LOEWE program of the State of Hesse and the Helmholtz Young Investigator Group No. VH-NG-332.

-
- [1] K. Fukushima and T. Hatsuda, Rept. Prog. Phys. **74**, 014001 (2011); K. Fukushima, arXiv:1108.2939 [hep-ph].
- [2] S. Leupold, K. Redlich, M. Stephanov, A. Andronic, D. Blaschke, *et al.*, Lect. Notes Phys. **814**, 39 (2011).
- [3] A. Bazavov *et al.*, arXiv:1111.1710 [hep-lat].
- [4] S. Borsanyi *et al.* (Wuppertal-Budapest), JHEP **09**, 073 (2010); Y. Aoki, Z. Fodor, S. D. Katz, and K. K. Szabo, Phys. Lett. **B643**, 46 (2006); Y. Aoki *et al.*, JHEP **06**, 088 (2009).
- [5] K. Fukushima, arXiv:1008.4322 [hep-ph].
- [6] Y. Aoki, G. Endrodi, Z. Fodor, S. D. Katz, and K. K. Szabo, Nature **443**, 675 (2006); S. Gupta, X. Luo, B. Mohanty, H. G. Ritter, and N. Xu, Science **332**, 1525 (2011); D. Son and M. Stephanov, Phys. Rev. D **70**, 056001 (2004).
- [7] O. Philipsen, arXiv:1111.5370 [hep-ph].
- [8] T. K. Herbst, J. M. Pawłowski, and B.-J. Schaefer, Phys. Lett. B **696**, 58 (2011).
- [9] J. Braun, L. M. Haas, F. Marhauser, and J. M. Pawłowski, Phys. Rev. Lett. **106**, 022002 (2011).
- [10] C. S. Fischer, J. Luecker, and J. A. Mueller, Phys. Lett. **B702**, 438 (2011).
- [11] T. Hatsuda, M. Tachibana, N. Yamamoto, and G. Baym, Phys. Rev. Lett. **97**, 122001 (2006); J.-W. Chen, K. Fukushima, H. Kohyama, K. Ohnishi, and U. Raha, Phys. Rev. **D80**, 054012 (2009); N. Yamamoto, M. Tachibana, T. Hatsuda, and G. Baym, Phys. Rev. **D76**, 074001 (2007).
- [12] M. Aggarwal *et al.* (STAR Collaboration), Phys. Rev. Lett. **105**, 022302 (2010); J. Adams *et al.* (STAR), Nucl. Phys. **A757**, 102 (2005).
- [13] B. Mohanty, Nucl. Phys. **A830**, 899c (2009).
- [14] V. Koch, arXiv:0810.2520 [nucl-th].
- [15] X. Luo, B. Mohanty, H. G. Ritter, and N. Xu, arXiv:1105.5049 [nucl-ex].
- [16] M. A. Stephanov, K. Rajagopal, and E. V. Shuryak, Phys. Rev. **D60**, 114028 (1999); Phys. Rev. Lett. **81**, 4816 (1998).
- [17] S. Jeon and V. Koch, Phys. Rev. Lett. **85**, 2076 (2000); arXiv:hep-ph/0304012 [hep-ph].
- [18] S. Ejiri, F. Karsch, and K. Redlich, Phys. Lett. **B633**, 275 (2006).
- [19] B. Berdnikov and K. Rajagopal, Phys. Rev. **D61**, 105017 (2000).
- [20] M. A. Stephanov, Phys. Rev. Lett. **102**, 032301 (2009).
- [21] C. Athanasiou, K. Rajagopal, and M. Stephanov, Phys. Rev. **D82**, 074008 (2010).
- [22] R. V. Gavai and S. Gupta, Phys. Lett. **B696**, 459 (2011); M. Stephanov, Phys. Rev. Lett. **107**, 052301 (2011).
- [23] Y. Hatta and T. Ikeda, Phys. Rev. **D67**, 014028 (2003).
- [24] B.-J. Schaefer and J. Wambach, Phys. Rev. **D75**, 085015 (2007).
- [25] M. Wagner, A. Walther, and B.-J. Schaefer, Comp. Phys. Commun. **181**, 756 (2010).
- [26] D. Roder, J. Ruppert, and D. H. Rischke, Phys. Rev. **D68**, 016003 (2003); T. Herpay, A. Patkos, Z. Szepe, and P. Szepfalussy, Phys. Rev. **D71**, 125017 (2005); J. T. Lenaghan, D. H. Rischke, and J. Schaffner-Bielich, Phys. Rev. **D62**, 085008 (2000); O. Scavenius, A. Mocsy, I. N. Mishustin, and D. H. Rischke, Phys. Rev. **C64**, 045202 (2001); B.-J. Schaefer and H.-J. Pirner, Nucl. Phys. **A660**, 439 (1999); H. Meyer-Ortmanns and B.-J. Schaefer, Phys. Rev. **D53**, 6586 (1996).
- [27] K. Fukushima, Phys. Lett. **B591**, 277 (2004); P. N. Meisinger, T. R. Miller, and M. C. Ogilvie, Nucl. Phys. Proc. Suppl. **119**, 511 (2003); E. Megias, E. Ruiz Arriola, and L. L. Salcedo, Phys. Rev. **D74**, 065005 (2006); Phys. Rev. **D74**, 114014 (2006).
- [28] C. Ratti, M. A. Thaler, and W. Weise, Phys. Rev. **D73**, 014019 (2006).
- [29] B.-J. Schaefer, M. Wagner, and J. Wambach, Phys. Rev. **D81**, 074013 (2010); H. Mao, J. Jin, and M. Huang, J. Phys. **G37**, 035001 (2010); U. S. Gupta and V. K. Tiwari, Phys. Rev. **D81**, 054019 (2010); S. Chatterjee and K. A. Mohan, arXiv:1108.2941 [hep-ph].
- [30] R. D. Pisarski, Phys. Rev. **D62**, 111501 (2000); A. Dumitru and R. D. Pisarski, Phys. Lett. **B525**, 95 (2002).
- [31] B.-J. Schaefer and M. Wagner, Progress in Particle and Nuclear Physics **62**, 381 (2008).
- [32] B.-J. Schaefer, M. Wagner, and J. Wambach, PoS **CPOD2009**, 017 (2009); J. Wambach, B.-J. Schaefer, and M. Wagner, Acta Phys. Pol. B Proc. Suppl. **3**, 691 (2010).
- [33] S. Rößner, C. Ratti, and W. Weise, Phys. Rev. **D75**, 034007 (2007).
- [34] K. Fukushima, Phys. Rev. **D77**, 114028 (2008).
- [35] J. Braun, H. Gies, and J. M. Pawłowski, Phys. Lett. **B684**, 262 (2010).
- [36] B.-J. Schaefer, J. M. Pawłowski, and J. Wambach, Phys. Rev. **D76**, 074023 (2007).
- [37] J. Braun and H. Gies, Phys. Lett. **B645**, 53 (2007); JHEP **06**, 024 (2006).
- [38] B.-J. Schaefer, arXiv:1102.2772 [hep-ph]; J. M. Pawłowski, AIP Conf. Proc. **1343**, 75 (2011).
- [39] B.-J. Schaefer and M. Wagner, Phys. Rev. **D79**, 014018 (2009).
- [40] J. O. Andersen, R. Khan, and L. T. Kyllingstad, arXiv:1102.2779 [hep-ph].
- [41] V. Skokov, B. Friman, E. Nakano, K. Redlich, and B.-J. Schaefer, Phys. Rev. **D82**, 034029 (2010).
- [42] U. S. Gupta and V. K. Tiwari, arXiv:1107.1312 [hep-ph].
- [43] A. Andronic, P. Braun-Munzinger, and J. Stachel, Phys. Lett. **B673**, 142 (2009).
- [44] L. McLerran and R. D. Pisarski, Nucl. Phys. **A796**, 83 (2007).
- [45] R. B. Griffiths and J. Wheeler, Phys. Rev. **A**, 1047 (1970).
- [46] Y. Hatta and T. Ikeda, Phys. Rev. **D67**, 014028 (2003).
- [47] P. Costa, C. A. de Sousa, M. C. Ruivo, and H. Hansen, Europhys. Lett. **86**, 31001 (2009).
- [48] Y. Hatta and M. A. Stephanov, Phys. Rev. Lett. **91**, 102003 (2003).
- [49] R. Kubo, J. Phys. Soc. Jpn **17**, 1100 (1962).
- [50] W.-j. Fu and Y.-l. Wu, Phys. Rev. **D82**, 074013 (2010).
- [51] M. Cheng *et al.*, Phys. Rev. **D79**, 074505 (2009).
- [52] F. Karsch and K. Redlich, Phys. Lett. **B695**, 136 (2011).
- [53] F. Karsch, B.-J. Schaefer, M. Wagner, and J. Wambach, Phys. Lett. **B698**, 256 (2011); PoS **Lattice 2011**, 219 (2011).
- [54] R. V. Gavai and S. Gupta, Phys. Rev. **D71**, 114014 (2005); Phys. Rev. **D78**, 114503 (2008).

- [55] C. R. Allton, M. Doering, S. Ejiri, S. J. Hands, O. Kaczmarek, F. Karsch, E. Laermann, and K. Redlich, Phys. Rev. **D71**, 054508 (2005).
- [56] M. Asakawa, S. Ejiri, and M. Kitazawa, Phys. Rev. Lett. **103**, 262301 (2009); K. Redlich, B. Friman, and V. Skokov, Prog.Theor.Phys.Suppl. **186**, 485 (2010).
- [57] S. Mukherjee, J. Phys. **G38**, 124022 (2011).
- [58] L. Kumar, Nucl.Phys. **A862-863**, 125 (2011).
- [59] A. Griewank and A. Walther, *Evaluating Derivatives: Principles and Techniques of Algorithmic Differentiation*, 2nd ed. (SIAM, Philadelphia, 2008).
- [60] B. Friman, F. Karsch, K. Redlich, and V. Skokov, Eur. Phys. J. **C71**, 1694 (2011).
- [61] E. Nakano, B.-J. Schaefer, B. Stokic, B. Friman, and K. Redlich, Phys.Lett. **B682**, 401 (2010).
- [62] B.-J. Schaefer and J. Wambach, Nucl. Phys. **A757**, 479 (2005).
- [63] R. D. Pisarski and F. Wilczek, Phys. Rev. **D29**, 338 (1984).
- [64] C. Schmidt, Prog.Theor.Phys.Suppl. **186**, 563 (2010).